HHS Public Access

Author manuscript

Biochemistry. Author manuscript; available in PMC 2018 March 14.

Published in final edited form as:

Biochemistry. 2017 March 14; 56(10): 1536–1545. doi:10.1021/acs.biochem.6b01152.

Electrostatic Interactions as Mediators in the Allosteric Activation of Protein Kinase A RIα

Emília P. Barros[†,‡], **Robert D. Malmstrom**[†,‡], **Kimya Nourbakhsh**[†], **Jason C. Del Rio**[§], **Alexandr P. Kornev**[§], **Susan S. Taylor**[†,§], and **Rommie E. Amaro**[*,†,‡]

[†]Department of Chemistry and Biochemistry, University of California, San Diego, La Jolla, California 92093, United States

[‡]National Biomedical Computation Resource, University of California, San Diego, La Jolla, California 92093-0446, United States

[§]Department of Pharmacology, University of California, San Diego, La Jolla, California 92093, United States

Abstract

Close-range electrostatic interactions that form salt bridges are key components of protein stability. Here we investigate the role of these charged interactions in modulating the allosteric activation of protein kinase A (PKA) via computational and experimental mutational studies of a conserved basic patch located in the regulatory subunit's B/C helix. Molecular dynamics simulations evidenced the presence of an extended network of fluctuating salt bridges spanning the helix and connecting the two cAMP binding domains in its extremities. Distinct changes in the flexibility and conformational free energy landscape induced by the separate mutations of Arg239 and Arg241 suggested alteration of cAMP-induced allosteric activation and were verified through *in vitro* fluorescence polarization assays. These observations suggest a mechanical aspect to the allosteric transition of PKA, with Arg239 and Arg241 acting in competition to promote the transition between the two protein functional states. The simulations also provide a molecular explanation for the essential role of Arg241 in allowing cooperative activation, by evidencing the existence of a stable interdomain salt bridge with Asp267. Our integrated approach points to the role of salt bridges not only in protein stability but also in promoting conformational transition and function.

Graphical abstract

[*]Corresponding Author: ramaro@ucsd.edu. Phone: +1 (858) 534-9629.

Author Contributions: E.P.B. and R.D.M. contributed equally to this work.

ORCID: Rommie E. Amaro: 0000-0002-9275-9553

Supporting Information: The Supporting Information is available free of charge on the ACS Publications website at DOI: 10.1021/acs.bio-chem.6b01152.

Notes: The authors declare the following competing financial interest(s): R.E.A. is a co-founder of Actavalon, Inc., and a consultant for Apogen, Inc.

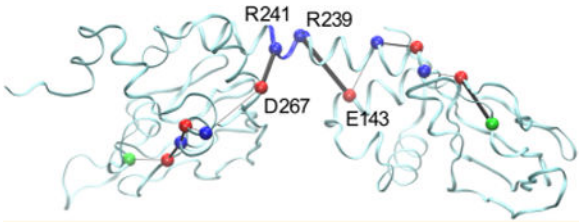

Protein structure is essential for protein function and is a result of interactions between neighboring as well as spatially distant residues relative to their primary sequence. Among the wide range of possible intra- and intermolecular interactions, salt bridges are defined by noncovalent charged interactions between acidic and basic residues[1] and are critical to the folding, stability, and function of most proteins.[2–5] Salt bridges are also key interactions in areas such as drug design and protein engineering.[6–8] In addition to playing important roles in structural stability, salt bridges can also mediate protein conformational change, allostery, and dynamics.[9,10]

The majority of the studies of salt bridges have involved static representations of biomolecules using structures resolved by X-ray crystallography. Molecular dynamics (MD) simulations, however, provide a means of studying these proteins at a dynamic and molecular level. As a model system for the investigation of the role of salt bridges in protein structure and function using all-atom MD simulations, we turned to the flexible type Iα regulatory subunit (RIα) of cAMP-dependent protein kinase A (PKA). The use of MD simulations coupled with experiments has recently successfully allowed the identification of allosteric networks on other protein kinases.[11–13]

PKA is a ubiquitous protein kinase that is important in many key cellular signaling pathways.[14] In its basal state, PKA exists in an inactive holoenzyme conformation containing a regulatory (R) subunit dimer and two catalytic (C) subunits and is activated by the second-messenger cyclic adenosine monophosphate (cAMP).[15] The R subunits bind to cAMP cooperatively and allosterically activate the holoenzyme by unleashing the catalytically active C subunits.[16] All four R subunit isoforms (RIα and -β and RIIα and -β) share a conserved domain architecture, containing two tandem cyclic nucleotide binding domains (CBD-A and CBD-B) connected via a long helical segment, known as the B/C helix.[17] The B/C helix incorporates portions of both CBDs, including the αB and αC helices from CBD-A and the αN helix from the N3A motif of CBD-B.[18] The binding of cAMP and release of C are associated with a dramatic conformational change in R, with residues in the CBDs moving up to 30 Å from their position in the holoenzyme conformation.[14] The two conformations are termed the “H conformation” and “B conformation”, with the former being the holoenzyme and the latter bound to cAMP.

The B/C helix plays a critical role in the regulation of PKA activity and is proposed to be essential for allosteric signal transduction.[19,20] Several major structural changes occur in this helix upon protein activation. In the four R subunit isoforms, a conserved patch of four positively charged residues is located in the center of this important structural motif (Figure 1),[17,21–23] and mutational studies of Arg241 showed it to be important for cooperative

activation.[24] While differences in some PKA mutant's dynamics and function have been attributed to disruptions in individual salt bridges within R,[24,25] no systematic study has investigated the role of salt bridge networks in the function and stability of the RIα subunit. We therefore sought to evaluate the role of the positively charged basic patch within the B/C helix in the allosteric activation of PKA, using alanine mutagenesis to analyze the dynamic formation (or disruption) of salt bridge networks through MD simulations and validated by experimental *in vitro* activation assays.

With this aim, we have performed molecular dynamics simulations of the wild type and four mutants of RIα (R239A, K240A, R241A, and K242A) in the absence of the catalytic subunit and cAMP. The apo state was simulated to provide a molecular level view of the dynamics of RIα between its two structurally characterized states. We discuss the general features of the systems observed in the trajectories, including the flexibility of the B/C helix, and the differences in R conformational ensembles upon introduction of the mutations. In conjunction with *in vitro* fluorescence polarization assays, our results provide insights into the intrinsic flexibility of R and indicate that the basic patch in the B/C helix is important for stabilization of the H conformation and in governing conformational dynamics and allosteric regulation. Our analysis also suggests the existence of an extended electrostatic network connecting the two cAMP binding domains, with the Arg241–Asp267 and Arg239–Glu143 salt bridges in particular playing key roles in the activation and stabilization of PKA. Finally, this work constitutes another example of the role of close-range electrostatic interactions in the stabilization and function of macromolecules.

Materials and Methods

System Setup

The heavy atom coordinates for the five systems (wild type and mutants R239A, K240A, R241A, and K242A) of PKA RIα were obtained from the crystallographic structure of the holoenzyme (Protein Data Bank entry 2QCS[14]), ranging from residue 113 to 379, which omits the flexible dimerization/docking domain (residues 11–61), the inhibitory site (residues 94–98), and linker regions.[15] Residues were protonated at pH 7.0 using Maestro-integrated PROPKA and mutations made using Schrödinger's Maestro (version 10.4, Schrödinger, LLC, New York, NY). The proteins were solvated in water boxes with counterions and 150 mM NaCl to simulate physiological conditions. The Amber14SB[26] force field was used for the protein and NaCl with TIP3P waters.[27]

Molecular Dynamics Simulations

Simulations were performed using GPU-accelerated Amber 14.[26] The system was minimized in four stages: proton only, solvent, solvent and side chains, and the full system totaling 11,000 cycles using a combination of steepest decent and conjugate gradient methods. Equilibration involved an initial heating to 100 K at constant volume for 50 ps followed by heating to 310K at constant pressure, 1 bar, for 200 ps. The system was further equilibrated at 310 K and 1 bar for 750 ps. Molecular dynamics simulations were run as an ensemble with periodic boundary conditions at 1 bar and 310 K. We used a nonbonded short-range interaction cutoff of 10 Å, and the long-range electrostatic interactions were

approximated by particle mesh Ewald.[28] The simulations used a 2 fs time step with the SHAKE algorithm to constrain hydrogen atoms. Each protein system was simulated in five parallel runs of 1,000 ns each, each run being assigned new starting velocities, resulting in 5 μs of total sampling time for each system (Table S1).

Trajectory Analysis

Trajectories were visualized using VMD.[29] Structures obtained in the trajectory were aligned the β barrel of CBD-A (residues 152–225) and frames sampled for analyses every 100 ps. Secondary structure assignment and pairwise distance calculation for the salt bridge analysis were performed using functions from MDTraj,[30] and all other analysis involved in-house programs. For the secondary structure analysis, bootstrapping sampling was done in order to obtain estimates of the variances of alpha helical proportions among the systems. A total of 20000 bootstrapping samplings were performed, in each of which 1000 frames of the simulation were randomly selected. The secondary structure averages of each bootstrapping sampling were then used to create the histograms. The salt bridge distance cutoff was taken as a nitrogen–oxygen distance of 4 Å.

Data Sharing

All MD input files, MD trajectories, and ipython notebooks used for the analyses presented in the paper are available for download at http://doi.org/10.6075/J07D2S2X.

Purification of Regulatory Subunits and Generation of Mutants

The basic patch mutants (R239A, K240A, R241A, and K242A) were generated using QuickChange site-directed mutagenesis. Wild-type and mutant RIα proteins were purified as previously described.[16,31] Proteins were expressed in *Escherichia coli* BL21 (DE3) from Novagen for 20–24 h at 15 °C in TB medium. In brief, ammonium sulfate precipitation of the soluble lysate supernatants was batch bound overnight to a cAMP resin to purify via affinity chromatography. Proteins were eluted from the resin, using 40 mM cGMP, and applied to a Superdex 200 gel filtration column for final purification in gel filtration buffer [50 mM MES (pH 5.8), 200 mM NaCl, 2 mM EGTA, 2 mM EDTA, and 5 mM DTT].

Fluorescence Polarization Allosteric Activation Assay

Allosteric activation of type Iα PKA holoenzyme basic patch mutants was evaluated using a fluorescence polarization assay as previously described.[31] PKA holoenzymes were formed *in vitro* using a 1.2:1 (RIα:C) molar ratio in FP assay buffer [50 mM MOPS (pH 7.0), 35 mM NaCl, 10 mM $MgCl_2$, 0.005% (v/v) Triton X-100, 1 mM ATP, and 1 mM DTT]. The PKA inhibitory peptide conjugated to the 5/6-carboxyfluorescein (5/6-FAM-IP20) fluorophore was added to wells containing the PKA holoenzyme at a final concentration of 2 nM. The C subunit concentration was kept constant at 12 nM and titrated with various concentrations of cAMP (from 0 to 8000 nM) to induce dissociation and allow binding of 5/6-FAM-IP20 to the C subunit. After incubation for 30 min to reach equilibrium, fluorescence polarization (excitation at 485 ± 20 nm, emission at 535 ± 25 nm) was measured using a GENios Pro microplate reader (TECAN) in black, flat bottom 96-well low-binding polypropylene assay plates (Greiner). Three independent experiments were

performed, with each measurement being the mean of triplicate samples ± the standard deviation. Graphs were generated and analyzed in GraphPad Prism 7.0a (GraphPad, La Jolla, CA), using a sigmoidal dose–response curve of variable slope.

8-[Fluo]-cAMP Fluorescence Polarization Binding Assay

The ability of the R subunit basic patch mutants to bind cAMP in the absence of the C subunit was tested using the fluorescent cAMP analogue, 8-[fluo]-cAMP (Biolog), used at a final concentration of 10 nM. Wells were titrated with a range of R subunit concentrations (from 0 to 125 nM), which were diluted with FP assay buffer. Polarization readings were measured and analyzed as described above.

Results

Wild-Type Conformational Dynamics

The wild-type and mutant systems were simulated in five parallel runs of 1 μs each. Despite the time scales being shorter than those of the majority of biologically relevant processes, such as protein folding and domain mobility, we nonetheless observed great flexibility of the R subunit. To quantify this flexibility, we aligned all of the frames to the relatively rigid β barrel of CBD-A in the H conformation and measured the displacement of the center of mass of CBD-B relative to the principal moments of inertia of CBD-A's β barrel using spherical coordinates. In this new reference system, the distance between the centers of mass of CBD-A and CBD-B is given by d, and the displacement in the $x-y$ plane and relative to the z axis are given by angles ϕ and θ, respectively (Figure 2A).

The histogram of distances between the CBD's centers of mass for the wild-type system provides one measure of the flexibility of the system (Figure 2B). Most of the structures sampled adopted distances similar to that of the crystallo-graphic H conformation, which was also the initial position of our simulations. Interestingly, we found a great proportion of configurations that extended beyond the known B and H conformations' CBDs distances. Larger distances were observed, as well as a small fraction of conformations with the centers of mass of the two lobes even closer together than in the globular, collapsed B conformation.

The spherical angles describe the orientation of the B domain and enrich the three-dimensional quantification of the RIα conformational ensemble. We performed principal component analysis (PCA) on the coordinates sampled and found that the first two principal components are very similar to the chosen spherical angles (Figure S1). We thus extended our analysis using these spherical parameters because they provide a more intuitive representation of the ensemble, with the metrics directly indicating the relative position of CBD-A and CBD-B contrary to the more abstract representation given by principal components. With the most probable state being taken as a reference, the free energy landscape of the wild-type ensemble in terms of these two angles is shown in Figure 2C, as well as the values corresponding to the H and B crystallo-graphic conformations. On the time scale of the simulations, the transition between the H and B crystallographic conformations was not sampled, indicating that longer sampling would be required to observe the conformational change, as expected. However, this analysis shows that the most

probable wild-type apo R conformation, located at the well in Figure 2C, does not correspond to the crystallographic H conformation. It differs from the H conformation mainly by a rotation of the B/C helix, which results in a roughly 45°-rotated B domain relative to its position in the X-ray crystal structure (Figure 2E). The rotation of CBD-B in the apo conformation suggests an overlap with the C subunit position (Figure 2D); thus, we would not expect CBD-B to adopt this rotational position in the presence of the C subunit.

Mutant Conformational Ensembles

The spherical coordinate analysis was extended to the simulations of the four alanine mutations of the B/C helix basic patch. R239A, K240A, and K242A displayed behavior similar to that of the wild type in terms of the distance between the CBD's centers of mass, with the exception of a slight increase in the number of observed conformations that have more proximal lobes, or smaller values of d (Figure 3). R241A, however, showed an opposite trend, with no sampling of these more collapsed conformations and instead a significant number of structures in which the centers of mass were farther apart than in H.

The free energy landscape in terms of the spherical angles for the mutants is shown in Figure 4. Comparison with that of the wild type (Figure 2C) shows that the mutations of K240 and K242 did not significantly affect the sampled conformational ensemble of R, while the removal of basic residues R239 and R241 resulted in a markedly different distribution of structures and the sampling of novel conformations (see Figure S2). These conformations displayed dramatic bends and deformations of the B/C helix (Figure 5 and Figure S3) and were more regularly sampled than in the wild-type, K240A, and K242A simulations. These observations and the distribution of CBD distances suggest that, for R239A and R241A (especially the latter), there is uncoupling between the two domains upon the removal of the basic residue, resulting in much more freedom in conformational exploration. Nonetheless, all of these mutants still sample for a significant part of the simulations conformations similar to the wild-type's most probable conformation, as evidenced by the presence of the wells in the same values of ϕ and θ.

Flexibility of the B/C Helix

Visual inspection suggested a high degree of flexibility in the B/C helix for all systems (Figure 5). Analysis of the spherical coordinates provided an indirect indication of this flexibility, because the displacement of CBD-B relative to CBD-A's principal moments of inertia was mainly caused by movements in the B/C helix. To directly quantify the plasticity of the helix and identify regions with a greater propensity for deformation, we calculated the fraction of residues in the B/C helix (residues 226–250) that displayed an α-helical secondary structure at each analyzed frame (Figure 6A). The wild type, K240A, and K242A showed similar helix proportions, in agreement with the similarity in their conformational ensembles. The B/C helix in R239A and R241A was less well formed, having a lower helix proportion, as would be expected from the greater sampling of bent structures (Figure 5).

We further refined this analysis by calculating, for each residue in the helix, the fraction of frames in which it possesses an α-helical structure (Figure 6B). Most of the residues had very high helical proportions, with the notable exception of C-terminal residues Ser249 and

Lys250 [not shown in Figure 6B, with helical proportions ranging from 12.0 to 22.2% and from 3.8 to 11.0%, respectively (see Figure S4)]. These residues, in all of the systems, were assigned in the majority of the frames as hydrogen-bonded turns.[32] In addition, R239A and R241A showed smaller helical proportions for other residues in the helix Residues 226–236, located in the N-terminal part of the helix (in CBD-A), were less ordered in R239A, with Leu233 being the most flexible of these. Oppositely, for R241A, it was the C-terminal part of the helix, comprising residues 233–248 in CBD-A and CBD-B, which displayed the most pronounced flexibility. In this case, Leu238 had the greatest diversion from the wild-type and other mutants' helical proportion. Both Leu233 and Leu238 are found in the interface with the C subunit in the holoenzyme structure (Figure S5). Mutational studies of Leu233 have suggested that this residue is important for allowing the formation of the holoenzyme, with L233A displaying a 3-fold decrease in the cAMP activation constant and a 3-fold increase in the R–C dissociation constant.[19]

Allosteric Activation and cAMP Binding of B/C Helix Mutants

MD simulations suggested that mutations of the arginine residues of the basic patch induce perturbations in the dynamics and conformational ensemble of the R subunit. Given the dependence of enzyme function on protein structure and the overall shape of the free energy landscape, the observations described above implicated altered function of R239A and R241A compared to wild-type RIα.

To validate our MD simulations of the basic patch mutants, we used two separate *in vitro* fluorescence polarization assays to address binding of cAMP to R subunits and allosteric activation of holoenzyme complexes (Figure S6). We initially speculated that because the mutations do not directly interact with cAMP in either the H or B conformation, cAMP binding would not be significantly impacted. As expected, using a fluorescent cAMP analogue, 8-[fluo]-cAMP, we found only minor differences in K_d values for R239A and K242A compared to that of wild-type RIα, with no change in cooperativity for any mutant (Table 1 and Figure S6a). We assessed the allosteric activation of PKA using an assay to measure dissociation of the C subunit from mutant holoenzyme complexes in response to increasing concentrations of cAMP, by measuring polarization of the fluorescent 5/6-FAM-IP20 peptide that binds to the free C subunit in solution (Table 1 and Figure S6b). As anticipated, we found that R241A was >20-fold less sensitive to cAMP-stimulated activation and less cooperative than the wild type, but R239A was slightly more sensitive to cAMP and exhibited greater cooperativity. Furthermore, K240A, but not K242A, showed a modest decrease in sensitivity to cAMP with no change in cooperativity.

Discussion

The use of all-atom MD simulations evidenced the pronounced flexibility of the apo regulatory subunit of PKA. Free wild-type PKA adopts a variety of conformations, with the extended, crystallographic H conformation being only rarely sampled (Figure 2). Instead, a structure with a slight torsion on the B/C helix constitutes the most probable conformation, which disrupts the C subunit binding interface (Figure 2E). This finding suggests that the

binding to C and inactivation of the enzyme require straining of the B/C helix and the R subunit undergoing the transition into a mechanically “frustrated” state.

The protein frustratometer Web server (frustratometer.tk)[33] was used to support this hypothesis, and the contact interactions in the B/C helix are predicted to be frustrated compared to the energetics of other residues in the same location [mutational frustration (Figure S7a)] or the same interactions in other configurations [configurational frustration (Figure S7b)].[34] This structural frustration of R in the holoenzyme provides a molecular explanation for the quick activation of PKA upon cAMP binding and its ability to act as a dynamic allosteric switch. Despite favorable interactions in the R–C interface, the strain in the B/C helix favors the release of C and may be one of the factors that results in the shallow free energy landscape observed using long timescale MD simulations and Markov state models.[20]

Mutation of Arg239 or Arg241 to alanine greatly perturbs the conformational ensemble of the regulatory subunit. R241A, in particular, differs from the other systems in that the CBD's dynamics seem to be decoupled, resulting in conformations in which they are separated by large distances. Similarly, the greatest variations in helix flexibility, as measured by the helix proportion, were seen in the R239A and R241A simulations. Our analysis further allowed the identification of the areas in the B/C helix that have a stronger propensity to be deformed and found that Leu233 in the case of R239A and Leu238 in R241A, both located at the interface with the catalytic subunit, are the most affected residues.

To relate the observed mutationally driven perturbation of the ensembles of R239A and R241A to the role of the basic residues and their involvement in electrostatic interactions, we calculated the total survival time of all of the salt bridges established within RIα from the simulations. This metric corresponds to the total fraction of frames in the simulation in which each salt bridge is formed. A qualitative representation of the network of salt bridges in the wild type is given in Figure 7A. The great majority of the salt bridges are intradomain, formed exclusively within CBD-A and within CBD-B. Interestingly, the only stable interdomain salt bridge, formed for approximately 80% of the time in the wild-type simulation, is between Arg241 and Asp267. The same calculation was performed for the mutants, and the total survival times of salt bridges that showed a change of >10% compared to that of the wild type are shown in Figures S8–S11.

The survival times of the salt bridges in the mutant systems indicate that the disruption of a very reduced number of salt bridges by a single mutation affects a variety of others, emphasizing the fact that there is communication between the charged residues throughout RIα and that they are involved in an extended network. Moreover, the mutations in Arg239 and Arg241 involved deletion of stable, long-lived stable salt bridges, while Lys240A and Lys242A removed only transient, short-lived interactions. Using the identified salt bridges in the simulations, an electrostatic network can be established from the cAMP binding site in domain A, extending through the B/C helix and reaching CBD-B (Figure 7B).

Arg241–Asp267 functions as the main interdomain salt bridge, allowing communication between the two binding sites. Crystal structures of the cAMP-bound R subunit and previous

structural models have suggested that PKA activation involved an interaction between Glu200 and Arg241, with Glu200 interacting with the 2′-hydroxyl group in cAMP.[24] Our simulations of the wild type and mutants, however, did not sample the B conformation, with Arg241 and Glu200 not coming into close contact with each other. Our analysis therefore shows that there is no such salt bridge formed between these residues, indicating instead that the decoupling of the two domains happens because of the breakage of the Arg241–Asp267 salt bridge. The loss of allosteric activation seen experimentally is therefore a result of the removal of the interdomain interaction, which breaks the electrostatic communication between the CBDs and disrupts the propagation of the allosteric signal.

The fluorescence polarization assays, on the other hand, indicate that Arg239 is involved in interactions of a different nature, contributing to the stability of the regulatory subunit in the extended, H-like conformation. The increased level of R–C dissociation may be caused by the destabilization of the binding interface, particularly Leu233, resulting in an effect similar to that of the L233A mutation.[19] In this way, the salt bridges involving Arg239 may function as “anchors” to keep the helix extended and allow the formation of the binding interface.

The coupling of computational and experimental analysis suggests that Arg239 and Arg241 play competing roles and that their modulation is an important factor for the regulation of PKA. We propose, in this way, that the extended salt bridge network is a key component of the allosteric mechanism and that there is a mechanical aspect to the conformational change caused by activation, with the salt bridges exerting a torque on the flexible B/C helix More specifically, Arg239 and Arg241 seem to have essential roles in the stabilization of the H conformation and in the allosteric transduction upon activation, respectively.

In conclusion, the investigation of the dynamics of ion pair interactions in PKA using MD simulations and experimental assays allowed the identification of several complex salt bridges and how they modulate the dynamics and function of PKA. Because there is compensation between the electrostatic interactions and variations in the pairs throughout the simulations due to side chain flexibility and greater-scale multidomain motion, the use of computer simulations to investigate these interactions can greatly enrich the structural or ensemble-averaged observations achieved with other methods.

Supplementary Material

Refer to Web version on PubMed Central for supplementary material.

Acknowledgments

This work was funded in part by the National Institutes of Health (NIH) through the NIH Director's New Innovator Award Program (DP2-OD007237 to R.E.A. and R01-GM034921 to S.S.T.) and a National Science Foundation (NSF) XSEDE supercomputer resources grant (RAC CHE060073N to R.E.A.). Funding from the National Biomedical Computation Resource (NBCR), NIH Grant P41 GM103426, is gratefully acknowledged. J.C.D.R was supported in part by the UCSD Graduate Training Program in Cellular and Molecular Pharmacology through an institutional training grant from the National Institute of General Medical Sciences (T32 GM007752).

References

1. Kumar S, Nussinov R. Close-Range Electrostatic Interactions in Proteins. ChemBioChem. 2002; 3:604–617. [PubMed: 12324994]
2. Tissot AC, Vuilleumier S, Fersht AR. Importance of two buried salt bridges in the stability and folding pathway of Barnase. Biochemistry. 1996; 35:6786–6794. [PubMed: 8639630]
3. Elcock AH, McCammon JA. Electrostatic contributions to the stability of halophilic proteins. J Mol Biol. 1998; 280:731–748. [PubMed: 9677300]
4. Jonsdottir LB, Ellertsson BO, Invernizzi G, Magnusdottir M, Thorbjarnardottir SH, Papaleo E, Kristjánsson MM. The role of slat bridges on the temperature adaptation of aqualysin I, a thermostable subtilisin-like proteinase. Biochim Biophys Acta, Proteins Proteomics. 2014; 1844:2174–2181.
5. Zíma V, Witschas K, Hynkova A, Zímová L, Barvík I, Vlachova V. Structural modeling and patch-clamp analysis of pain-related mutation TRPA1-N855S reveal inter-subunit salt bridges stabilizing the channel open state. Neuropharmacology. 2015; 93:294–307. [PubMed: 25724085]
6. Cui G, Freeman CS, Knotts T, Prince CZ, Kuang C, McCarty NA. Two salt bridges differentially contribute to the maintenance of cystic fibrosis transmembrane conductance regulator (CFTR) channel function. J Biol Chem. 2013; 288:20758–20767. [PubMed: 23709221]
7. Bairagya HR, Mukhopadhyay BP, Bera AK. Role of salt bridge dynamics in inter domain recognition of human IMPDH isoforms: an insight to inhibitor topology for isoform-II. J Biomol Struct Dyn. 2011; 29:441–462. [PubMed: 22066532]
8. Makhatadze GI, Loladze VV, Ermolenko DN, Chen X, Thomas ST. Contribution of surface salt bridges to protein stability: Guidelines for protein engineering. J Mol Biol. 2003; 327:1135–1148. [PubMed: 12662936]
9. Gur M, Madura JD, Bahar I. Global transitions of proteins explored by a multiscale hybrid methodology: application to adenylate kinase. Biophys J. 2013; 105:1643–52. [PubMed: 24094405]
10. Zhang L, Buck M. Molecular simulations of a dynamic protein complex: Role of Salt-bridges and polar interactions in configurational transitions. Biophys J. 2013; 105:2412–2417. [PubMed: 24268153]
11. Shukla D, Meng Y, Roux B, Pande VS. Activation pathway of Src kinase reveals intermediate states as targets for drug design. Nat Commun. 2014; 5:3397. [PubMed: 24584478]
12. Foda ZH, Shan Y, Kim ET, Shaw DE, Seeliger MA. A dynamically coupled allosteric network underlies binding cooperativity in Src kinase. Nat Commun. 2015; 6:5939. [PubMed: 25600932]
13. Lu S, Deng R, Jiang H, Song H, Li S, Shen Q, Huang W, Nussinov R, Yu J, Zhang J. The mechanism of ATP-dependent allosteric protection of Akt Kinase phosphorylation. Structure. 2015; 23:1725–1734. [PubMed: 26256536]
14. Kim C, Cheng CY, Saldanha SA, Taylor SS. PKA-I Holoenzyme Structure Reveals a Mechanism for cAMP-Dependent Activation. Cell. 2007; 130:1032–1043. [PubMed: 17889648]
15. Boettcher AJ, Wu J, Kim C, Yang J, Bruystens J, Cheung N, Pennypacker JK, Blumenthal Da, Kornev AP, Taylor SS. Realizing the allosteric potential of the tetrameric protein kinase A RIα holoenzyme. Structure. 2011; 19:265–76. [PubMed: 21300294]
16. Su Y, Dostmann RG, Herberg FW, Durick K, Xuong Nh, Ten Eyck L, Taylor S, Varughese KI. Regulatory Subunit of Protein Kinase A: Structure of Deletion Mutant with cAMP Binding Domains. Science (Washington, DC, U S). 1995; 269:807–813.
17. Bruystens JGH, Wu J, Fortezzo A, Kornev AP, Blumenthal DK, Taylor SS. PKA RIa homodimmer structure reveals an intermolecular interface with implications for cooperative cAMP binding and carney complex disease. Structure. 2014; 22:59–69. [PubMed: 24316401]
18. Kornev AP, Taylor SS, Ten Eyck LF. A generalized allosteric mechanism for cis-regulated cyclic nucleotide binding domains. PLoS Comput Biol. 2008; 4:e1000056. [PubMed: 18404204]
19. Sjoberg TJ, Kornev AP, Taylor SS. Dissecting the cAMP-inducible allosteric switch in protein kinase A RIalpha. Protein Sci. 2010; 19:1213–21. [PubMed: 20512974]
20. Malmstrom RD, Kornev AP, Taylor SS, Amaro RE. Allostery through the computational microscope: cAMP activation of a canonical signalling domain. Nat Commun. 2015; 6:7588. [PubMed: 26145448]

21. Wu J, Brown SHJ, von Daake S, Taylor SS. PKA type IIa holoenzyme reveals a combinatorial strategy for isoform diversity. Science (Washington, DC, U S). 2007; 318:274–279.
22. Zhang P, Smith-Nguyen EV, Keshwani MM, Deal MS, Kornev AP, Taylor SS. Structure and allostery of the PKA RIIβ tetrameric holoenzyme. Science (Washington, DC, U S). 2012; 335:712–716.
23. Ilouz R, Bubis J, Wu J, Yim YY, Deal MS, Kornev AP, Ma Y, Blumenthal DK, Taylor SS. Localization and quaternary structure of the PKA RIβ holoenzyme. Proc Natl Acad Sci U S A. 2012; 109:12443–12448. [PubMed: 22797896]
24. Symcox MM, Cauthron RD, Ogreid D, Steinberg RA. Arg-242 Is Necessary for Allosteric Coupling of Cyclic AMP-binding Sites A and B of RI Subunit of Cyclic AMP-dependent Protein Kinase. J Biol Chem. 1994; 269:23025–23031. [PubMed: 8083203]
25. Gibson RM, Ji-Buechler Y, Taylor SS. J Biol Chem. 1997; 272:16343–16350. [PubMed: 9195940]
26. Case, DA., Babin, V., Berryman, JT., Betz, RM., Cai, Q., Cerutti, DS., Cheatham, TE., III, Darden, TA., Duke, RE., Gohlke, H., Goetz, AW., Gusarov, S., Homeyer, N., Janowski, P., Kaus, J., Kolossváry, I., Kovalenko, A., Lee, TS., LeGrand, S., Luchko, T., Luo, R., Madej, B., Merz, KM., Paesani, F., Roe, DR., Roitberg, A., Sagui, C., Salomon-Ferrer, R., Seabra, G., Simmerling, CL., Smith, W., Swails, J., Walker, RC., Wang, J., Wolf, RM., Wu, X., Kollman, PA. AMBER 14. University of California; San Francisco: 2014.
27. Jorgensen WL, Chandrasekhar J, Madura JD, Impey RW, Klein ML. Comparison of Simple Potential Functions for Simulating Liquid Water. J Chem Phys. 1983; 79:926–932.
28. Darden TA, York D, Pedersen L. Particle-mesh Ewald: An N.log(N) method for Ewald sums in large systems. J Chem Phys. 1993; 98:10089–10092.
29. Humphrey W, Dalke A, Schulten K. VMD-Visual Molecular Dynamics. J Mol Graphics. 1996; 14:33–38.
30. McGibbon RT, Beauchamp KA, Harrigan MP, Klein C, Swails JM, Hernandez CX, Schwantes CR, Wang LP, Lane TJ, Pande VS. MDTraj: a modern open library for the analysis of molecular dynamics trajectories. Biophys J. 2015; 109:1528–1532. [PubMed: 26488642]
31. Wu J, Jones JM, Xuong NH, Ten Eyck LF, Taylor SS. Crystal structures of RIalpha subunit of cyclic adenosine 5′-monophosphate (cAMP)-dependent protein kinase complexed with (Rp)-adenosine 3′,5′-cyclic monophosphothioate and (Sp)-adenosine 3′,5′-cyclic monophosphothioate, the phosphothioate analogues of cA. Biochemistry. 2004; 43:6620–6629. [PubMed: 15157095]
32. Kabsch W, Sander C. Dictionary of protein secondary structure: pattern recognition of hydrogen-bonded and geometrical features. Biopolymers. 1983; 22:2577–2637. [PubMed: 6667333]
33. Parra RG, Schafer NP, Radusky LG, Tsai MY, Guzovsky AB, Wolynes PG, Ferreiro DU. Protein Frustratometer 2: a tool to localize energetic frustration in protein molecules, now with electrostatics. Nucleic Acids Res. 2016; 44:W356–W360. [PubMed: 27131359]
34. Jenik M, Parra RG, Radusky LG, Turjanski A, Wolynes PG, Ferreiro DU. Protein frustratometer: A tool to localize energetic frustration in protein molecules. Nucleic Acids Res. 2012; 40:W348–W351. [PubMed: 22645321]

Abbreviations

C subunit	catalytic subunit
cAMP	cyclic adenosine monophosphate
CBD	cyclic nucleotide binding domain
MD	molecular dynamics
NMR	nuclear magnetic resonance
PKA	cAMP-dependent protein kinase A

R subunit regulatory subunit

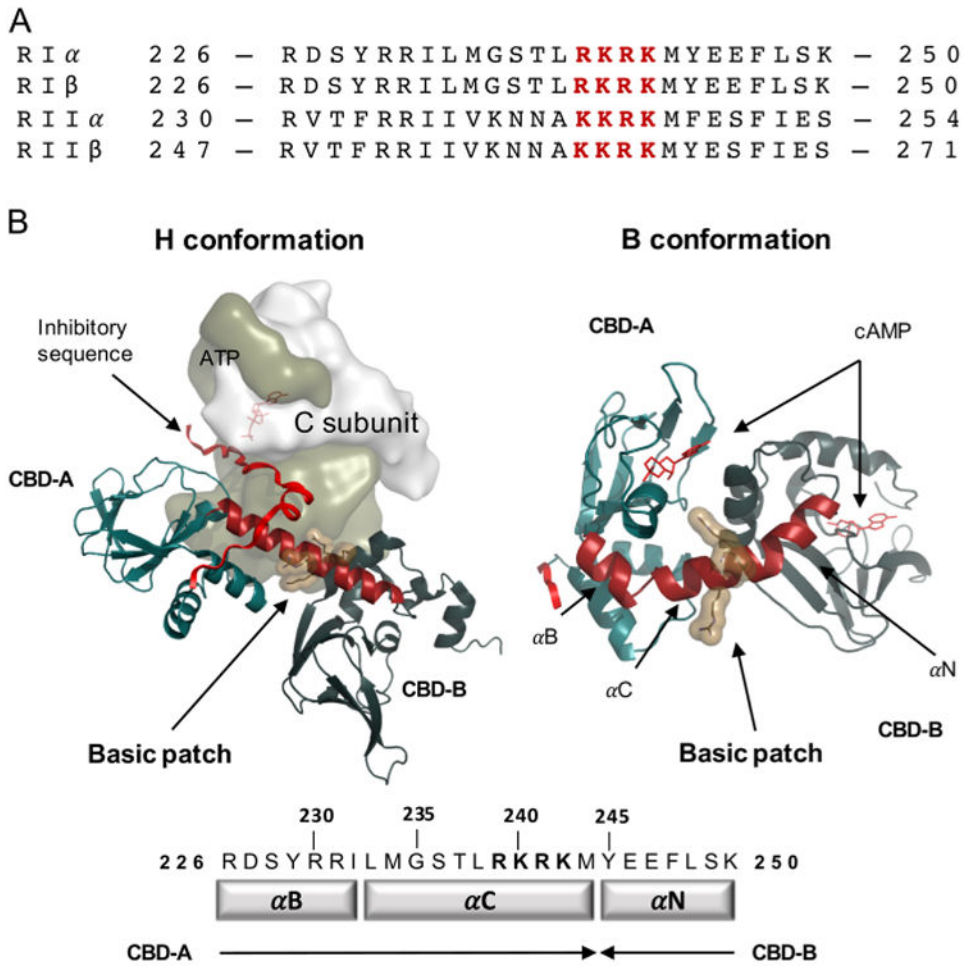

Figure 1.

(A) Sequence alignment of the B/C helix of the four isoforms of the regulatory subunit. The positive patch in the B/C helix is colored red. (B) Representation of the regulatory subunit and B/C helix conformation at the two functional conformations of PKA. The side chains of the basic patch residues are colored ochre, the B/C helix is colored red, the N lobe of the C subunit is colored white and the C lobe tan.

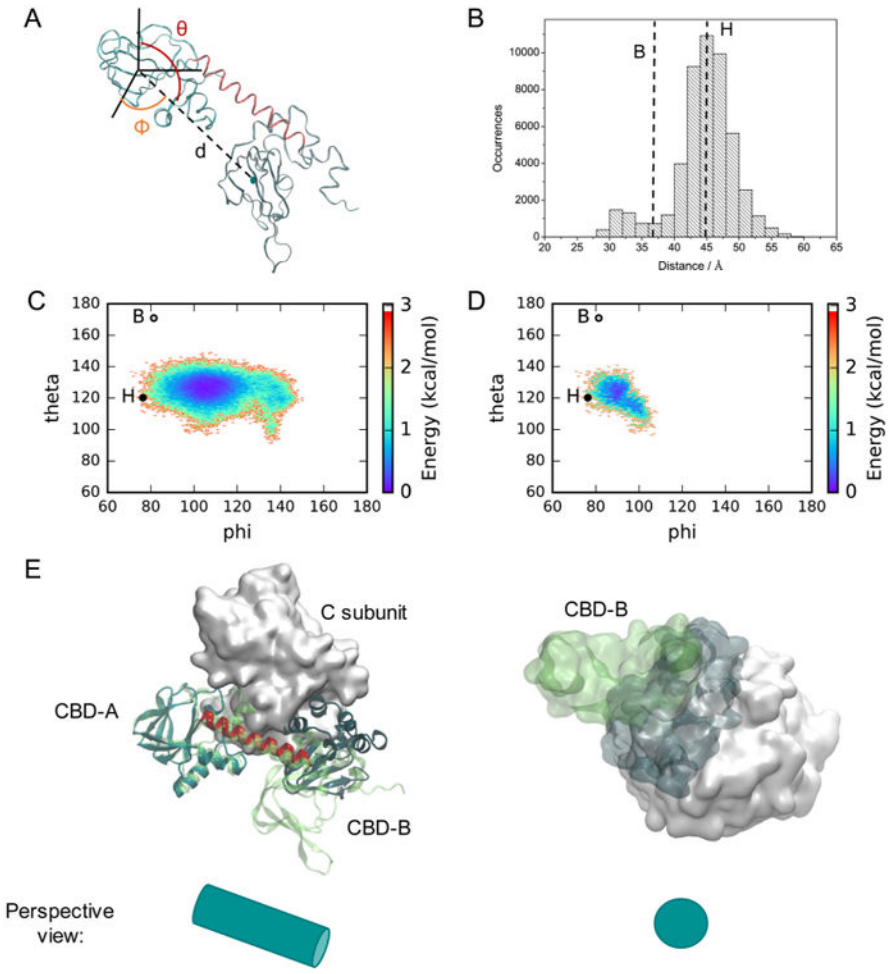

Figure 2.

Dynamics of the wild-type system. Spherical coordinate analysis of the conformational flexibility of wild-type RIα. (A) Representation of the spherical coordinates of the center of mass of the CBD-B β barrel relative to the principal moments of inertia of the H conformation CBD-A β barrel. (B) Histogram of the center of mass distances. (C) Free energy landscape in terms of spherical angles ϕ and θ for the complete set of sampled conformations. (D) Free energy landscape of the structures showing no overlap with the coordinates of the C subunit in the holoenzyme crystallographic structure. The spherical coordinates corresponding to the crystallographic structures are also shown. (E) Two views of the most probable conformation in the wild-type ensemble (CBD-A colored cyan, B/C helix red, and CBD-B dark green) compared to the crystallographic H conformation (regulatory subunit colored green and catalytic subunit white). Structures were aligned in their CBD-A β barrel.

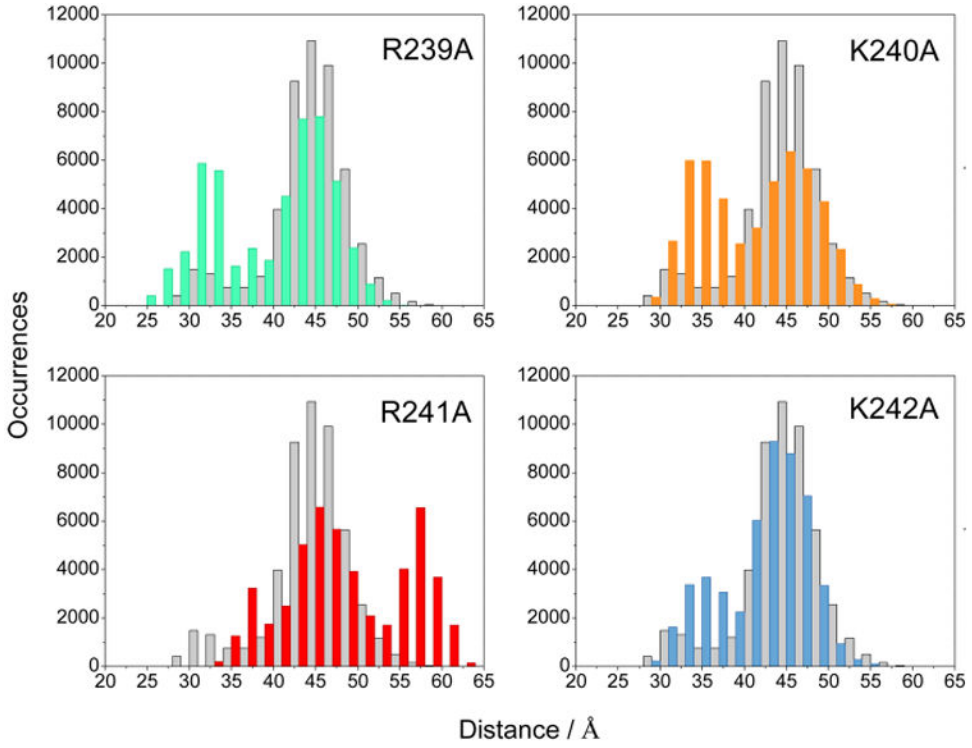

Figure 3.
Histogram of CBD's centers of mass distance for the mutants (colors) vs the wild type (gray).

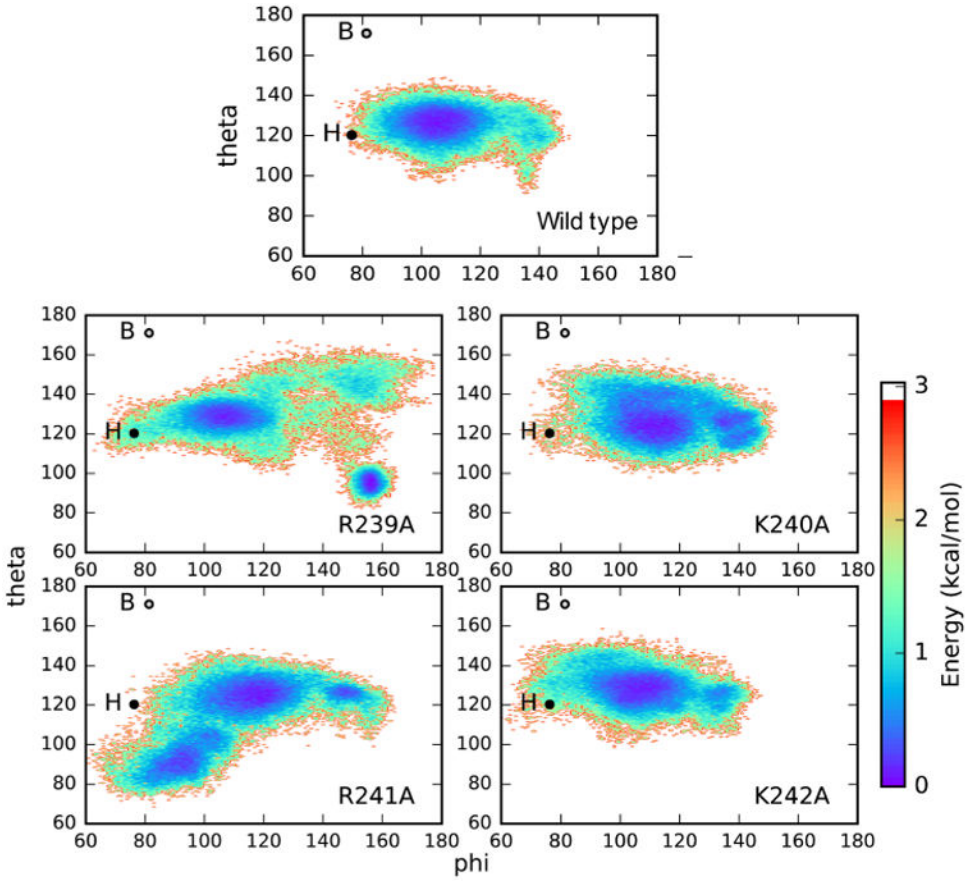

Figure 4.

Free energy landscape in terms of spherical angles for the wild type and mutants. The coordinates for the crystallographic structures are also shown.

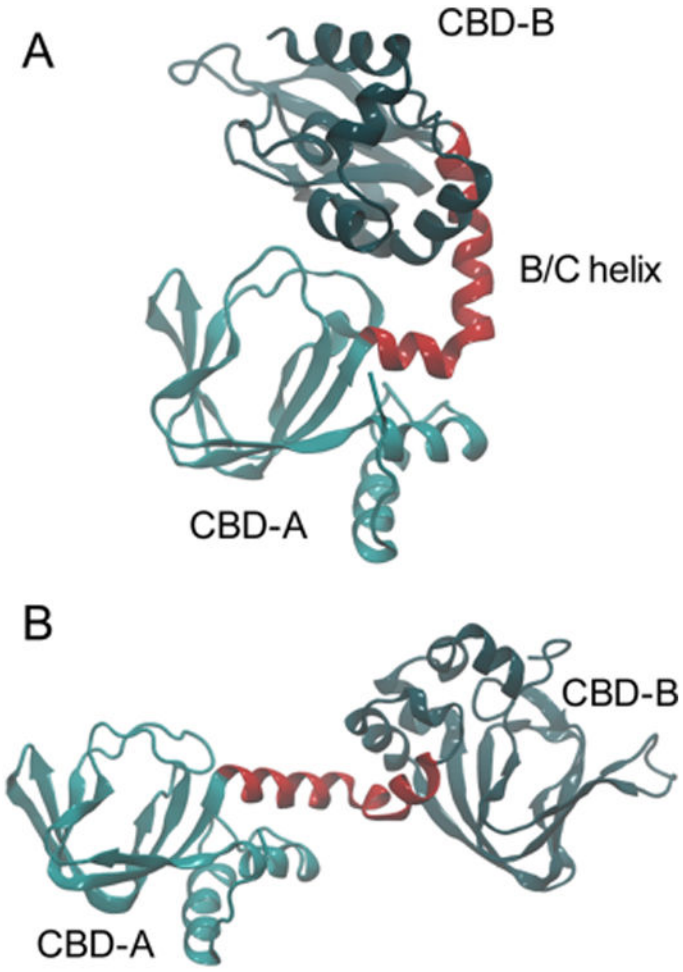

Figure 5.
Novel conformations sampled in (A) R239A and (B) R241A simulations. CBD-A is colored cyan, CBD-B dark green, and the B/C helix red.

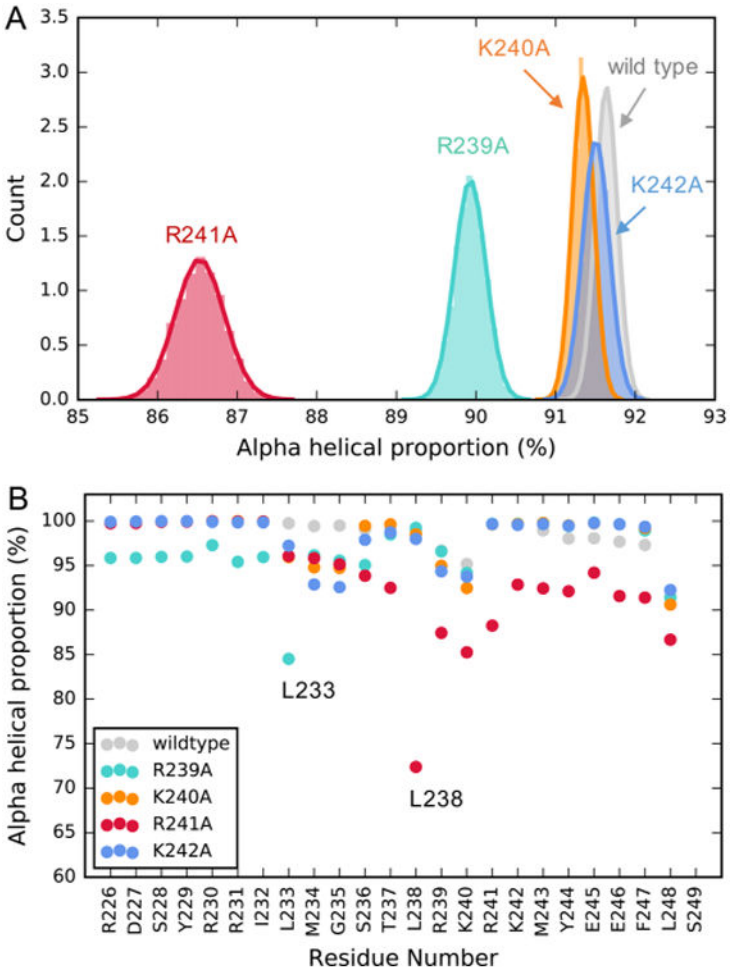

Figure 6.

B/C helical proportion analysis of wild-type and mutant systems. (A) Full helix analysis and (B) per-residue analysis for residues located in the B/C helix.

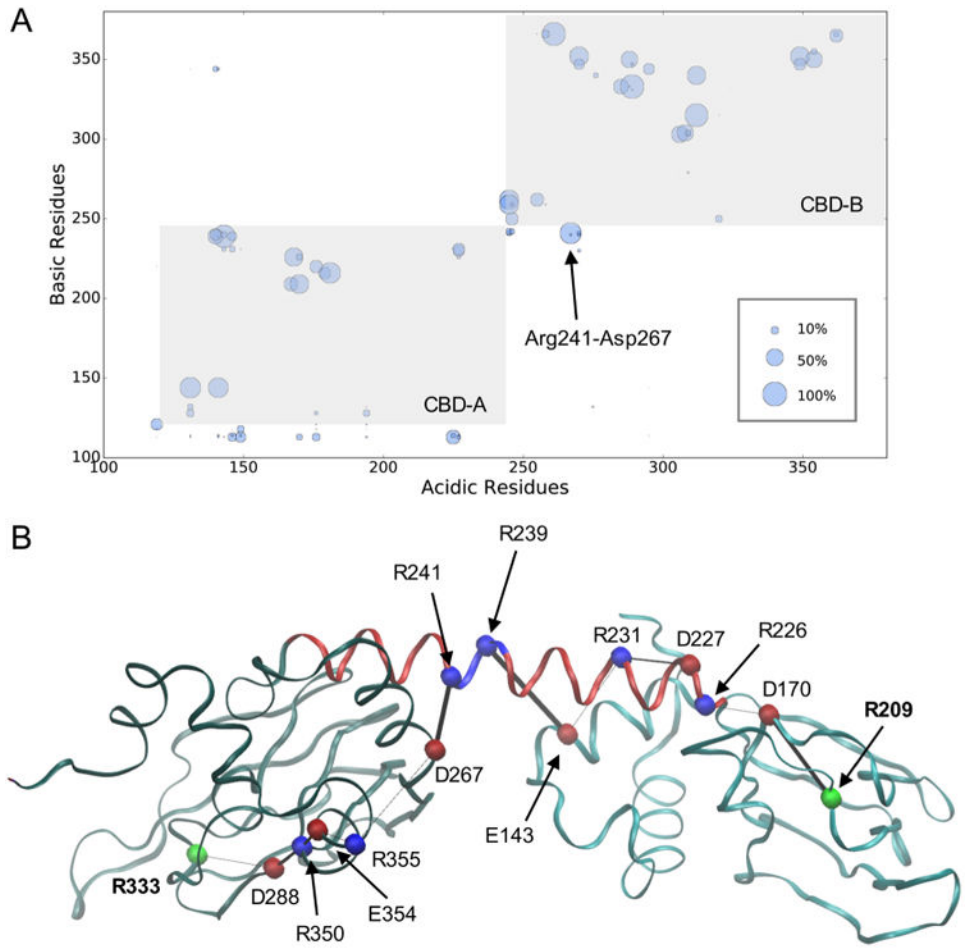

Figure 7.

Network of salt bridges. (A) Survival times of salt bridges formed in wild-type simulations. The size of the spheres is proportional to the total survival time of the salt bridge. (B) Scheme of an electrostatic network connecting the two cAMP binding domains. Basic residues are colored blue and acidic residues red, with the exception of residues in the cAMP binding sites, Arg209 and Arg233, which are colored green. The thickness of the black lines represents the lifetime of the salt bridge as measured in the wild-type simulation.

Table 1

Nucleotide Binding and Allosteric Activation of RIα B/C Helix Basic Patch Mutants and the Wild Type

	cAMP binding		activation of PKA	
system	K_d (nM)	Hill coefficient	EC_{50} (nM)	Hill coefficient
wild type	7.30 ± 0.11	1.65 ± 0.04	23.36 ± 0.66	2.11 ± 0.11
R239A	6.72 ± 0.11	1.71 ± 0.04	17.64 ± 0.67	2.54 ± 0.22
K240A	7.32 ± 0.12	1.83 ± 0.05	29.98 ± 1.23	2.15 ± 0.18
R241A	7.29 ± 0.10	1.80 ± 0.04	543.07 ± 27.40	1.44 ± 0.09
K242A	7.71 ± 0.11	1.80 ± 0.04	24.93 ± 0.85	1.86 ± 0.10